Strong three-dimensional correlations in the vortex system for $(Bi_{0.7}Pb_{0.3})_{2.2}Sr_2CaCu_2O_8$

L. S. Uspenskaya* and A. B. Kulakov
Institute of Solid State Physics, Russian Academy of Sciences, Chernogolovka, Moscow District, 142432, Russia

A. L. Rakhmanov†
Institute for Theoretical and Applied Electrodynamics, Russian Academy of Sciences, Izhorskaya Street 13/19, Moscow, 125412, Russia

(Received 5 November 2002; revised manuscript received 31 March 2003; published 9 September 2003)

An experimental study of magnetic flux penetration under crossed magnetic fields in Bi2212:Pb single crystals is performed by the magneto-optic technique. A remarkable field penetration pattern alteration and superconducting current anisotropy enhancement by the in-plane field is revealed. The anisotropy increases with the temperature rise up to $T_m = 54 \pm 2$ K. At $T = T_m$ an abrupt change in the flux penetration behavior is found. The correlation between the in-plane magnetic field and the out-of-plane magnetic flux penetration disappears and no correlation is observed at $T > T_m$. The transition temperature T_m does not depend on the magnetic field strength. The observed flux penetration anisotropy is considered as a evidence for a strong three-dimensional correlation between pancake vortices in different CuO planes at $T < T_m$. This enables the observation of a remarkable pinning in Bi2212:Pb at low temperatures.

DOI: 10.1103/PhysRevB.68.104506 PACS number(s): 74.72.Hs, 74.25.Ha

I. INTRODUCTION

The structure and dynamics of the magnetic flux in high-T_c superconductors (HTSC's) are intensively studied because of their importance for both fundamental physics and applications. The main results of these studies are summarized in several reviews.[1–3] The investigations reveal the variety of flux line lattice (FLL) states or phases in HTSC's. Peculiarities of the FLL structure are determined by the crystal symmetry or by the nature of pinning. The transitions between different FLL phases are possible with temperature and magnetic field variation. The qualitative difference in the FLL properties is found to be closely related to the layered structure of the crystal lattice of HTSC materials. In particular, the pancakelike and Josephson-like vortex structures are observed in an inclined magnetic field in highly anisotropic Bi- and Tl-based superconductors, whereas anisotropic Abrikosov vortices are found in superconductors with a lower anisotropy, such as YBCO. However, even in highly anisotropic superconductors the three-dimensional (3D) correlations can exist between the two-dimensional (2D) pancakelike vortices located in neighboring CuO planes.[1–3] The FLL behavior of such a 3D-correlated phase is in some aspects closer to the anisotropic Abrikosov vortex lattice than to an uncorrelated 2D phase. Basically, the 3D correlations in the pancake structure could disappear with an increase of temperature due to the first-order phase transition or FLL melting. The possibility of different types of FLL phase transitions in highly anisotropic HTSC's was widely discussed.[1–13]

The high resolution magneto-optic (MO) technique[14,15] is admitted to be a convenient tool for direct observation of the magnetic flux structure and dynamics in superconductors. In particular, MO studies in crossed magnetic fields are employed to clarify the presence or absence of 3D correlations in FLL's of superconductors.[8,9,16–21] In these experiments, a platelike specimen of a single crystal is placed in a dc magnetic field directed in the sample plane $\mathbf{H}_{ab}$ and then a field $\mathbf{H}_z$ perpendicular to the plane is applied. In such geometry the MO technique is used to study the penetration of the magnetic flux induced by the field $\mathbf{H}_z$. The experiments reveal two strikingly different types of flux behavior depending on the anisotropy of the material.[16] The transverse flux moves into the YBCO single crystals preferably along the direction of the in-plane magnetic field $\mathbf{H}_{ab}$. Quite the contrary, the transverse magnetic flux penetrates independent of the orientation of the in-plane magnetic field in the case of highly anisotropic Bi2212 superconductors. This difference can be readily understood.[16,22,23]

Two systems of orthogonal vortices evidently exist in the sample under the considered field configuration. The first one is induced by the in-plane field and the second one enters the crystal under the growing perpendicular field. In the case of moderate crystal anisotropy, both systems consists of mutually perpendicular Abrikosov vortices. It is rather evident that perpendicular flux lines moves easier along the in-plane vortices than across them, because the vortex intersection requires an additional driving force and an additional energy.[24] This mechanism is effective for Abrikosov-like vortices and insignificant for the pancakelike structures existing in highly anisotropic materials.

The second reason for the in-plane field induced anisotropy is related to the magnetic interaction between vortices. The motion of the transverse magnetic flux along the in-plane field induces the current in the direction perpendicular to the in-plane vortices. As a result, Lorentz force acts on the in-plane vortices and the critical current density j_{cp} of the corresponding screening current is determined by the pinning force. The vortex motion across the in-plane vortices induces the current flowing along them. In this case the Lorentz force is zero. Such magnetic flux and current configuration is usually referred to as the force-free one.[25] The critical current density j_{cf} is limited now by the specific FLL instabilities.[25–29] This current is usually remarkably higher than the current determined by pinning $j_{cf} \gg j_{cp}$. Thus, the current screening the flux motion along $\mathbf{H}_{ab}$ is much smaller than the current screening the motion across $\mathbf{H}_{ab}$. This

 ©2003 The American Physical Society

mechanism is important for Abrikosov vortices. It could also be effective for pancake structures in the case of strong enough correlation between the pancakes located in different CuO planes.

The absence of strong anisotropy of the magnetic flux penetration induced by the in-plane field does not mean that the pancakes and Josephson vortices are completely independent in Bi2212. A specific weak interaction is discussed widely[30,31] and verified by direct MO observation in a low magnetic field range.[8,9,17–21]

The transition between two types of magnetization behavior of superconductors in crossed fields is not reported in the literature. This transition could probably be observed in materials with intermediate anisotropies compared to YBCO and Bi2212. Possible ways to achieve the goal are to increase the anisotropy of the YBCO material by preparing oxygen-deficient samples or to reduce the anisotropy of the Bi2212 superconductor by Pb doping.

It is known[6,32–35] that Pb doping of Bi2212 single crystals reduces the electromagnetic anisotropy parameter $\gamma^2 = \rho_c / \sqrt{\rho_a \rho_b}$ from 8.5×10^3 to 2.5×10^3 with the Pb content varying from 0 to 0.3 as measured at $T=100$ K; here ρ_i denotes the normal resistivity along the corresponding crystal axis **i**. In addition, the doping significantly increases the critical current density that was attributed to the FLL pinning at so-called laminar superstructure formed by varying the Pb content in the system of planes parallel to the **ac** crystal plane.[35]

In the present work a penetration of the transverse magnetic flux into the Pb-doped Bi2212 single crystals magnetized by the in-plane magnetic field is studied by the MO technique in a wide temperature range, 12–91 K. We characterize the flux penetration qualitatively by the images and quantitatively by the profiles of the perpendicular magnetic induction $B_z(\mathbf{r})$ measured along different directions in the sample plane. We find that the in-plane magnetic field $\mathbf{H}_{ab}$ remarkably influences the transverse flux penetration pattern if the temperature T is lower than some threshold value $T_m = 54\pm2$ K. The growth of H_{ab} gives rise to the increase of the current anisotropy and causes the preferential flux propagation along its direction. The current along $\mathbf{H}_{ab}$ becomes stronger with H_{ab} while the current across the $\mathbf{H}_{ab}$ becomes weaker. The anisotropy induced by the in-plane field increases with the temperature rise.

The flux penetration behavior changes drastically at $T = T_m$. In the temperature range $T>T_m$ the penetration becomes independent of the in-plane field direction and the flux creep increases significantly. The transition temperature T_m is independent of the strength of the both magnetic fields H_{ab} and H_z within the studied ranges $0<H_{ab}<1800$ Oe and $0<H_z<300$ Oe. So, our samples behave similar to YBCO at temperatures below T_m and Bi2212 at higher temperatures.

II. SAMPLES

The single crystals of $(Bi_{0.7}Pb_{0.3})_{2.2}Sr_2CaCu_2O_{8+\delta}$ were grown by the top solution growth technique.[36,37] As-grown samples have platelike shapes with the main surface coinciding with the **ab** crystallographic plane. To provide the flat surface that is always necessary for MO studies, the samples were chemically polished in ethylendiaminetetraacetic acid. The final thickness of the samples was 70–100 μm. The inductive coil measurements show $T_c \approx 91$ K with a transition width of about 1 K. For the sake of clarity and comparison we present the MO images for one typical sample of trapezium shape in Fig. 1. Other crystals of different shapes exhibited similar results.

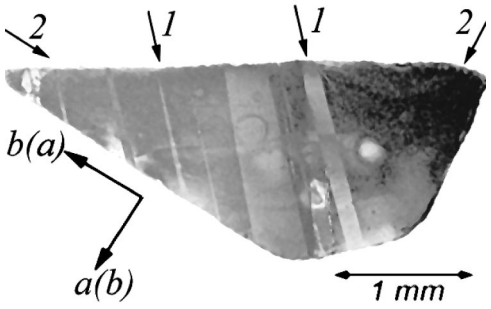

FIG. 1. Polarized light optical microscope image of the sample surface. Arrows show the directions of crystallographic axes (**a**,**b**), twin boundaries (1), and laminar structure (2). Twins are seen as light gray and dark gray stripes crossing the sample along the diagonal between **a**,**b** directions; the laminar structure is invisible.

The θ-2θ x-ray scanning revealed a structure typical for Bi2212:Pb planar defects, twins and laminae.[36,37] The twin boundaries are parallel to the **c** axis and coincide with the bisectrix of the angle between **a** and **b** axis. Twins are seen in the given polarized-light image as stripes with light and dark contrast, some of them are marked by arrows 1 in Fig. 1. The laminar structure is invisible in polarized light. The laminae are parallel to the nearest trapezium sides in Fig. 1 (their directions are marked by arrows 2).

III. EXPERIMENTAL

The MO studies were performed in a temperature range from 12 K to T_c. The distribution of the transverse magnetic induction $\mathbf{B}_z$ was observed by means of standard MO technique.[14,15,38] The indicator films used in the study allow us to correctly reconstruct the magnetic induction distribution in the transverse field H_z up to 2000 Oe. The MO images were taken by the EDC1000 digital video camera of fixed sensitivity and variable exposure. The brightness of the images is a function of magnetic induction. Benefiting from the constant film sensitivity within the temperature range 12–150 K we calibrated the brightness with respect to the induction value. For this purpose we recorded the MO images at given values of H_z and H_{ab} and at T slightly above T_c. These images were used as graduation marks for induction mapping at T below T_c. As a result, the profiles of the transverse magnetic induction along and across the applied in-plane magnetic field were obtained.

The transverse magnetic field $\mathbf{H}_z$ parallel to the crystal **c** axis was generated by a solenoidal coil. The value of H_z could be varied from 0 to ±1200 Oe. The in-plane magnetic field $\mathbf{H}_{ab}$ was produced by Helmholtz coils with a soft magnetic core. The uniformity of the field better than 1% was

attained across the sample. We were capable of rotating the field $\mathbf{H}_{ab}$ in any direction and changing its value from 0 to 1800 Oe. The orientation of this field with respect to the sample plane was controlled by the MO technique with an accuracy about 10^{-3} rad. The experiments were performed on samples cooled from room temperature either with or without $\mathbf{H}_{ab}$ (FC or ZFC regime, respectively).

IV. MAGNETOOPTIC OBSERVATIONS OF FLUX PENETRATION

A. Zero in-plane field

The transverse magnetic flux penetrates into the sample under the growing H_z through a few weak points, which are located at the positions where the twin boundaries intersect the sample edges, compare Figs. 1 and 2. The flux enters through the same points within the whole temperature range. The penetrated flux looks similar to bubbles attached to the sample edges, Figs. 2(a)–2(c). White spots in Fig. 2 correspond to the entered magnetic flux; the brighter the spot, the higher the induction.

With the increase of H_z the flux ''bubble'' expands and remains ''attached'' to the specimen edge. The same penetration depth is reached at lower fields with temperature growth. The aspect ration of the flux bubble is nearly the same at all temperatures below 54 K.

The localization of the entered flux near the weak point is favorable for the present study since the bubble's shape characterizes the anisotropy of the flux penetration in the **ab** plane. This anisotropy is remarkably smaller than expected from the data on the critical current anisotropy due to laminar structure in the literature.[34] In our experiments most of the observed flux bubbles show rather small anisotropy at a temperature below 54 K. Only the flux spot located close to the sharp corner of the sample has a pronounced flux penetration anisotropy, Fig. 2. However, this fact could be attributed to the influence of the Meissner current configuration near the corner.

The configuration of the entered magnetic flux is determined by the distribution of all screening currents in the sample. Thus, the flux penetration anisotropy only qualitatively characterizes the current anisotropy . The current distribution can be calculated from the magnetic induction map.[34,39] According to the Maxwell equation, the derivative of the induction taken in the direction normal to the flux front $\partial B_z/\partial \mathbf{r}$, is proportional to the tangent component of the current. The profiles $B_z(r)$ measured approximately along and across the laminar structure are given in Fig. 3 [corresponding directions are marked by arrows in Fig. 2(b)].

The magnetic induction in the bubble is a slowly varying function of coordinates near its center and decays almost linearly at the periphery. This linear part is used to characterize the current anisotropy.

The slope of $B_z(\mathbf{r})$ varies with direction which could be attributed to the flux pinning by the laminar structure. The angular dependence of $|\partial B_z/\partial r|$ is shown in Fig. 4 (curve 1); α is determined as the angle between the directions of vector $\mathbf{r}$ and perpendicular to the laminae, marked by arrow 1 in Fig. 2(b). So, the higher the $\partial B_z/\partial r$ in some direction, the higher the current J that flows in the perpendicular direction. We find that the current anisotropy does not exactly follow the direction of the laminar structure with a minimum current along the laminae and a maximum one across them. Both directions of minimum and maximum current are shifted by about 30° clockwise. The current anisotropy could be characterized by the coefficient k_J defined as the ratio of maxi-

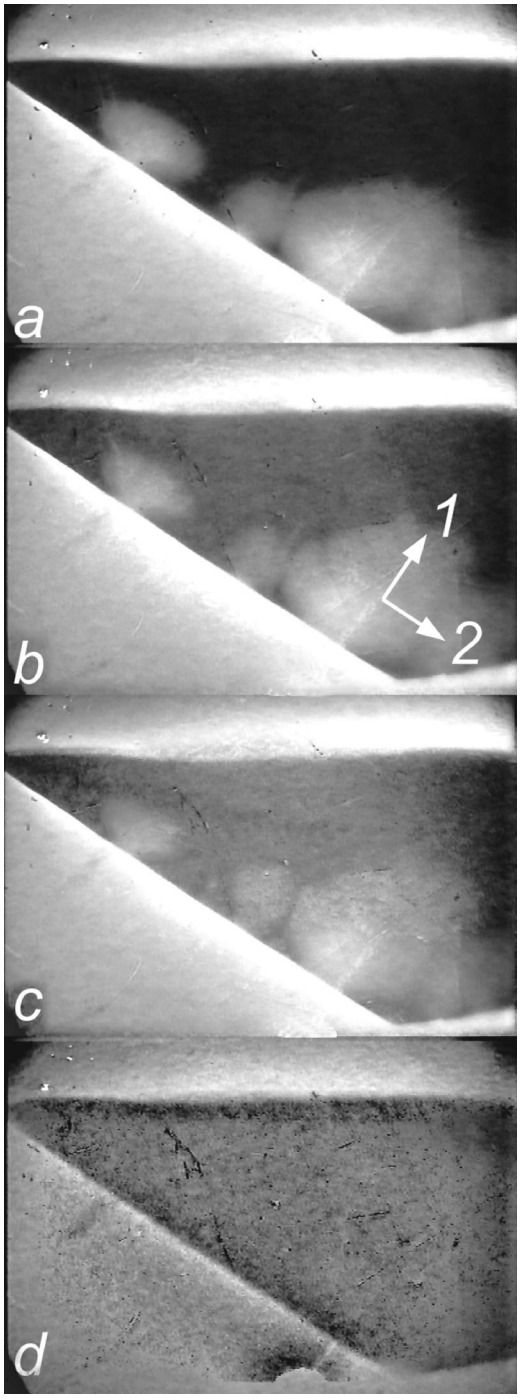

FIG. 2. MO images of the transverse magnetic field penetration at $H_{ab}=0$; (a) $T=24$ K, $H_z=149$ Oe, (b) $T=37$ K, $H_z=75$ Oe, (c) $T=51$ K, $H_z=46$ Oe, and (d) $T=54.5$ K. $H_z=34$ Oe, white arrows 1 and 2 indicate the directions across and along the laminar structure.

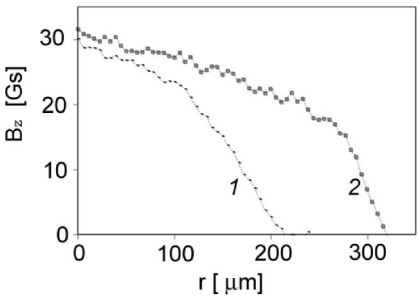

FIG. 3. Magnetic flux distribution $B_z(r)$ along two directions, marked by arrows 1 and 2 in Fig. 2(b). $H_z=38$ Oe, $H_{ab}=0$, $T=30$ K. The coordinate origin $r=0$ is chosen at the point with the maximum induction magnitude.

mum and minimum induction derivatives taken at the flux spot periphery $k_J=|(\partial B_z/\partial r)_{\max}/(\partial B_z/\partial r)_{\min}|$. The value of k_J does not exceed 2 in the temperature range from 12 to 50 K and in the field range $0<H_z<300$ Oe.

The magnetic field penetration behavior changes with the temperature, compare Figs. 2(a)–2(d). The flux bubbles remain attached to the corresponding entrance points while $T<T_m=54\pm2$ K. The separate bubbles with the definite $B_z(r)$ slopes could be made out at $T<T_m$ if H_z is not too high. The flux creep rate grows with temperature: the flux distribution is quasistable at $T=12$ K, the flux enters only a few percent deeper into the sample in ten minutes after H_z is turned on at $T=30$ K, and the flux spreads by 20% deeper in seconds at $T=51$ K.

At $T>T_m$, the flux penetration behavior changes drastically. The magnetic flux starts to penetrate the superconductor at the same weak points and spreads fast over the whole sample volume. Only frame by frame browsing of video records allows us to trace the flux behavior. We found that the flux moves fast towards some geometrical center of the sample. In the process of motion the separate bubbles run into and generate a smooth flux distribution shown in Fig. 2(d) in a time less than 0.1 s. The observed drop of the magnetic induction near the sample edges is due to the flux exclusion by the Meissner current. Such magnetic flux distribution is typical for undoped Bi2212.[16]

B. MO studies in crossed fields

The in-plane magnetic field $\mathbf{H}_{ab}$, changes the flux penetration pattern if $T<T_m$. The perpendicular magnetic flux

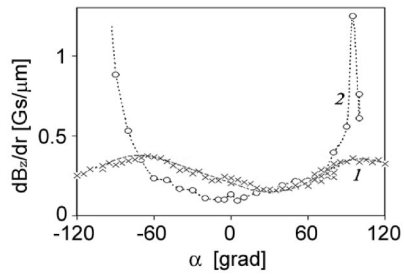

FIG. 4. Angular dependence of $|\partial B_z/\partial r|$ at $T=30$ K and $H_z=38$ Oe. Curves 1 and 2 are obtained at $H_{ab}=0$ and 1800 Oe, respectively. $\alpha=0$ corresponds to the direction across the laminar structure indicated by arrow 1 in Fig. 2(b).

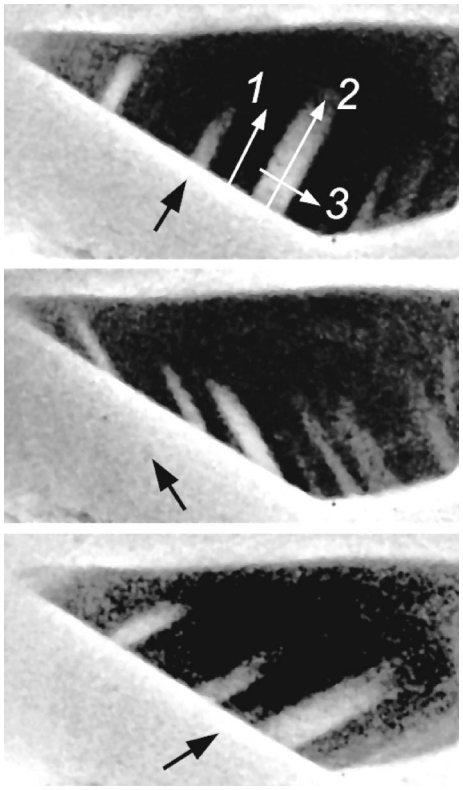

FIG. 5. MO images of the flux distribution in the case of the sample cooled in the in-plane field $H_{ab}=1800$ Oe ($H_z=60$ Oe and $T=30$ K). Different images correspond to different directions of $\mathbf{H}_{ab}$ indicated by black arrows. White arrows 1, 2, and 3 indicate the directions along which $B_z(r)$ profiles are given in Fig. 6.

enters the superconductor from the same weak points as in the absence of $\mathbf{H}_{ab}$. However, the flux moves predominantly along the direction of the vector $\mathbf{H}_{ab}$. For this reason, the entered flux looks similar to stripes extended along $\mathbf{H}_{ab}$.

Typical pictures of the transverse magnetic flux distribution in the presence of the in-plane field at $T<T_m$ and fixed H_z are shown in Fig. 5 (FC regime). Different images in the figure correspond to different directions of the vector $\mathbf{H}_{ab}$. The flux penetration depth and the magnetic induction magnitude rise with the increase of the transverse field H_z. The anisotropy of magnetic flux penetration increases monotonically with the growth of the in-plane magnetic field (the entered flux stripes become thinner and longer).

The appearance of the penetration anisotropy induced by the in-plane field in Bi2212:Pb was not reported until now. Such behavior of the magnetic flux is observed within the temperature range from 12 to 54 ± 2 K. This type of field penetration is analogous to that usually observed in YBCO single crystals.

In Fig. 6 three profiles of the magnetic field induction taken along the directions indicated in Fig. 5 by the white arrows are shown. Curve 1 is the coordinate dependence of B_z along the $\mathbf{H}_{ab}$ direction (**x** axis) measured between two weak points where the magnetic flux penetration is screened by the Meissner currents. Some growth of the magnetic field near the edge is due to the nonzero demagnetizing factor of the sample. Such a ''hill'' is always observed near the thin

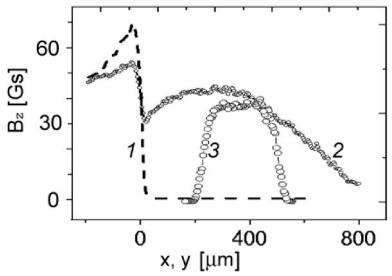

FIG. 6. Profiles of the magnetic field induction at $T=30$ K, $H_{ab}=650$ Oe, and $H_z=60$ Oe. Curve 1 is the induction profile along $\mathbf{H}_{ab}$ far from weak points, curve 2 and 3 are obtained near a weak point along and across the direction of in-plane field, respectively.

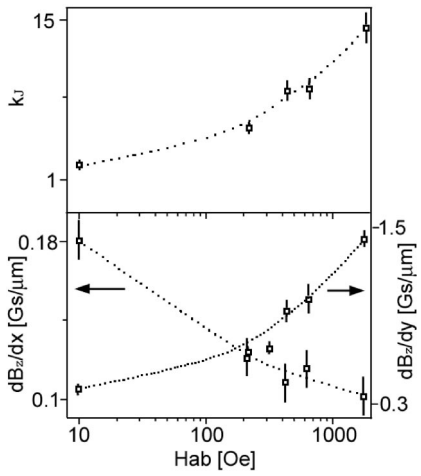

FIG. 7. Dependences $|\partial B_z/\partial x|$, $|\partial B_z/\partial y|$, and k_J vs H_{ab} for $T=30$ K and $H_z=77$ Oe.

crystal edge. Curve 2 is the magnetic induction profile $B_z(x)$ scanned in the same direction but near the weak point within the band of the magnetic flux penetration into the superconductor. This profile exhibits a definite drop near the surface due to the Meissner current. In the bulk of the sample, the entering magnetic flux has a variable slope similar to the case of $H_{ab}=0$ shown in Fig. 3. Namely, the field $B_z(x)$ varies slowly near the magnetic induction maximum and drops down almost linearly at the flux periphery. Profile 3 is obtained in the same flux penetration zone as profile 2 but in the direction perpendicular with respect to the vector $\mathbf{H}_{ab}$ ($\mathbf{y}$ axis). This profile also consists of parts with different slopes, that is, the central part with a small flux gradient and two peripheral parts with the much steeper and almost linear slopes. The value of the transverse slope $\partial B_z/\partial y$ is much larger than the longitudinal one $\partial B_z/\partial x$ and both of them are much smaller than the slope of the magnetic induction due to the Meissner current.

The application of the in-plane field changes considerably the gradient of the magnetic induction $\partial B_z/\partial r$ at the flux bubble periphery. The corresponding angle dependence of $\partial B_z/\partial r$ measured in the same manner as in the case of $\mathbf{H}_{ab}=0$, is shown in Fig. 4 (curve 2). The curve is obtained at $T=30$ K and $H_{ab}=1800$ Oe under FC conditions. The $\mathbf{H}_{ab}$ is directed along the laminae. The value of $\partial B_z/\partial r$ has a minimum precisely along this direction and increases sharply along the perpendicular one. It is evident that the in-plane field induced anisotropy is much stronger than the anisotropy due to the laminar structure.

The magnetic induction profiles change with the change of the in-plane field as well as the screening currents, which are proportional to the induction slopes. The induction derivative along the in-plane field decreases with H_{ab} while the derivative across this direction increases, Fig. 7. Hence, the x component of the current $J_{sx}(H_{ab})$ is an increasing function while the y component $J_{sy}(H_{ab})$ is a decreasing one. Accordingly, the current anisotropy coefficient k_J is an increasing function of H_{ab}, Fig. 7. So, the screening currents in Bi2212:Pb behave with the change of in-plane field in the same manner as in YBCO (Ref. 16) if $T<T_m$.

The magnetic flux penetration depth grows monotonically with T in the temperature range $12\ \mathrm{K}<T<T_m$, Fig. 8. We define the coefficient of geometrical anisotropy of the flux penetration k as a ratio of the maximum to minimum length of the entering flux stripe. It is evident from the images shown in Fig. 8 that k increases with T. The analysis of the magnetic induction profiles $B_z(r)$ reveals that the current anisotropy k_J is a growing function of temperature as well despite the decrease of both current components J_{sx} and J_{sy} with temperature, Fig. 9. It is seen that k and k_J increase with temperature approaching a saturation at $T\approx 40-45$ K for $k(T)$ and $25-30$ K for $k_J(T)$.

The picture of the magnetic field penetration changes dramatically if temperature exceeds the transition value T_m [see Fig. 8(d)] just as in the case of $H_{ab}=0$. The flux motion becomes independent of the in-plane magnetic field direction. The vortex lines enter the sample through weak points in the same way as at lower temperatures, but move to the particular ''geometric center.'' The position of this center is determined by the sample shape only and does not depend on the direction and the value of the in-plane field. The magnetic flux fills the sample volume in a time less than 0.04 s. Browsing of the MO frame sequence allows us to reveal the direction of the magnetic flux motion indicated by the white arrows in Fig. 8. Such a mode of flux penetration in crossed fields is similar to that observed in Bi2212 single crystals. The final distribution of vortices in our samples at $T>T_m$ is also similar to Bi2212 with a typical dome shape determined by the geometric barrier. It should be emphasized that the crossover temperature $T_m=54\pm 2$ K is independent of the magnetic field within the studied field ranges $H_{ab}=0-1800$ Oe and $H_z=0-300$ Oe.

Among the studied samples there were crystals with the same Pb doping but without twins. The magnetic flux enters such samples in a wide pillowlike front. The in-plane magnetic field influences the flux penetration pattern and magnetic induction slopes. The strong anisotropy induced by the in-plane field was observed in these samples only at $T<T_m$ and disappears at higher temperatures. We do not discuss the corresponding results since the MO images and magnetic induction profiles obtained for the crystals with weak points presented above are much more demonstrative and impres-

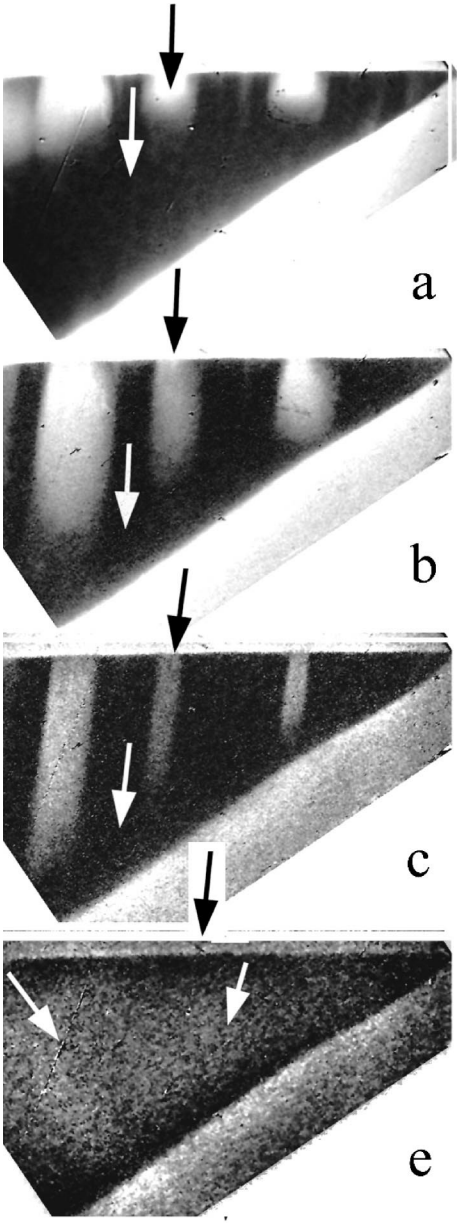

FIG. 8. MO images at $H_{ab}=1800$ Oe and different temperatures: (a) $T=17$ K and $H_z=302$ Oe, (b) 29 K and 154 Oe, (c) 43 K and 54 Oe, (d) 56 K and 40 Oe. Black arrows show the in-plane magnetic field direction, white arrows indicate the preferable direction of magnetic flux motion.

sive. The described above behavior of the magnetic flux in the FC regime is similar to the picture of the magnetic field penetration in the ZFC mode.

V. DISCUSSION

A. Magnetic flux dynamics below T_m

The MO studies in crossed fields reveal that supercurrents of three different types screen the magnetic flux entering into the sample. The largest current (see curve 1 in Fig. 6) flows near the sample surface far from the weak points. It can be associated with the Meissner current J_{sm}. The current density J_{sm} is independent of the in-plane magnetic field and an order of magnitude higher than two other currents J_{cx} and J_{cy} flowing in the sample bulk along and across the direction of the vector $\mathbf{H}_{ab}$, $J_{cy} \ll J_{cx} \ll J_{sm}$. Naturally, the values of the screening currents J_{sm}, J_{cx}, and J_{cy} decrease with temperature.

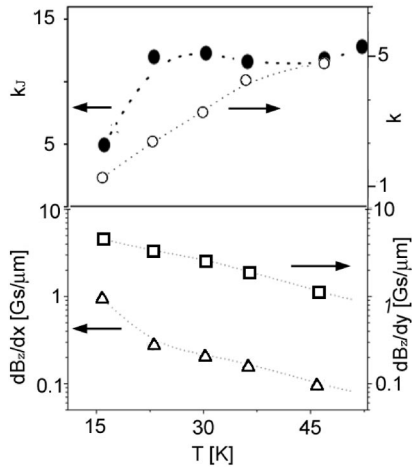

FIG. 9. Dependences $|\partial B_z/\partial x|$, $|\partial B_z/\partial y|$, k_J, and k vs T at crossed fields $H_{ab}=1800$ Oe and $H_z=77$ Oe.

We observed that $J_{cx} \propto |\partial B_z/\partial y|$ grows monotonically with H_{ab}, Fig. 7. In fact, the current along the in-plane field does not act by the Lorentz force on the in-plane vortices, as discussed in the Introduction. In such a force-free configuration the critical current density should increase with the increase of magnetic field.[25] The current across the in-plane field $J_{cy} \propto |\partial B_z/\partial x|$ decreases with H_{ab} as one often observes for pinning controlled current.

The geometric anisotropy and the current anisotropy increase with the temperature while $T<T_m$, Fig. 9. Such anisotropy growth was found for YBCO single crystals.[16] This could be related to the increase of superconducting coherence lengths with T. As a result, the superconducting correlations between different CuO planes become stronger giving rise to a stronger interaction between the in-plane and transverse magnetic fluxes.

The presented results show that at $T<T_m$ the magnetic properties of our samples are in many features analogous to those of YBCO. This allows us to assume the existence of rather strong 3D correlations in the vortex system of Bi2212:Pb.

B. FLL phase above T_m and transition temperature

The apparent picture of the magnetic flux penetration changes drastically at $T=T_m$. The observed disappearance of the intercoupling between the in-plane and transverse magnetization could find a reasonable explanation in terms of a decay of correlations between pancakes located in different CuO planes.[16,22,40] A possible explanation of the crossover in magnetization behavior at $T=T_m$ is vortex depinning and, then, $T_m(B)$ should be treated as an irreversibility line. Really, the flux creep rate rises and the pinning diminishes with T approaching T_m. However, the crossover temperature

T_m is independent of the magnetic field, while the magnetic field dependence of the irreversibility line is usually strong for Bi-based systems.[10–13] Moreover, at the crossover point the correlation between the direction of the entering transverse magnetic flux and the in-plane field decays in a steplike manner, which cannot be understood in terms of thermal depinning. At the same time, the decay of 3D correlations in the flux line system should be supplemented by the reduction of bulk pinning and by the disappearance of correlations between the transverse and in-plane flux. Therefore, we consider the 3D-2D crossover as a more realistic explanation of the observed transition at $T=T_m$.

Such a type of 3D-2D transition could occur due to melting of the vortex structure during which strongly correlated stacks of pancakes melt into a disordered gas or liquid of 2D vortices.[1–3] An indication that the observed change in FLL properties at T_m is due to some first-order phase transition is the behavior of the magnetic flux penetration anisotropy versus temperature. The anisotropy increases with T and reduces abruptly at $T=T_m$. The transition of the pancake stacks into the phase of noncorrelated 2D vortices should lead to a considerable increase of the thermal creep, e.g., due to diminishing of the activation volume and due to corresponding decrease of the effective pinning[3] that is observed in the experiment.

Following common conceptions,[2] the melting temperature T_m can be estimated by equating the characteristic energies of the FLL elastic strain and thermal fluctuations k_BT, where k_B is Boltzmann's constant. The corresponding relation is given by

$$k_BT_m = a_L C_{66} a_0^2 d_c, \tag{1}$$

where $a_L \ll 1$ is Lindeman's constant, C_{66} is the FLL shear modulus, a_0 is the FLL constant, and d_c is an effective correlation length between the pancakes along the **c** axis.[41,42] The value of d_c is of the order of the distance between neighboring CuO planes in strongly anisotropic system.[2] The melting temperature T_m defined by Eq. (1) is independent of the perpendicular magnetic field B_z since $a_0 \propto 1/\sqrt{B_z}$ and $C_{66} \propto B_z$.[1–3] The last fact is in agreement with the results of the present experiments. In the dislocation melt approach, Lindeman's constant can be estimated as $a_L = 1/4\pi$.[41] Substituting $C_{66} = B_z\phi_0/(4\pi\lambda_{ab})^2$ and $a_0^2 = 2\phi_0/\sqrt{3}B$ into Eq. (1) one finds the equation for the melting temperature[2,42]

$$k_BT_m = \phi_0^2 d_c/32\sqrt{3}\pi^2\lambda_{ab}^2(T_m), \tag{2}$$

where ϕ_0 is the magnetic flux quantum and $\lambda_{ab}(T)$ is the London penetration depth in the **ab** plane. We find $T_m \approx 50$ K if $d_c = 1-2$ nm and $\lambda_{ab}(0) = 200-300$ nm, which seems reasonable for Bi2212:Pb.[35,36] This estimation is not a strong proof but some evidence in favor of the 3D-2D transition.

In the disordered 2D phase the correlation between the motion of the transverse flux and the in-plane magnetic field is significantly lower compared to the 3D correlated system. The reduction of the activation volume makes easier the thermoactivated motion of the noncorrelated 2D vortices in any direction.

VI. CONCLUSION

The MO studies of Bi2212:Pb single crystals in crossed magnetic fields revealed that a transition occurs in the magnetic flux behavior at $T=T_m=54\pm2$ K. The transverse magnetic flux at $T<T_m$ behaves similar to YBCO spreading preferably along the in-plane magnetic field. At $T>T_m$ the transverse flux penetrates independent of the in-plane magnetic field as in the Bi2212 system. The anisotropy of the flux penetration increases with the in-plane magnetic field and temperature at $T<T_m$. The transition temperature is independent of the magnetic field. The obtained experimental results could be understood within the concept of the flux line melting giving rise to the transition of 3D correlated stacks of pancakes into disordered phase of 2D ones. We believe that the existence of strong 3D correlations in the flux line structure due to Pb doping is the main reason for enhanced critical current in Bi2212:Pb system.

ACKNOWLEDGMENTS

The authors acknowledge M. V. Indenbom, V. V. Riazanov, L. M. Fisher, I. F. Voloshin, A. V. Kalinov, I. K. Bdikin, K. I. Kugel for useful discussions, and the Alexander von Humboldt Foundation for financial support for part of the experimental equipment. This work was supported by INTAS (Grant No. 01-2282), RFBR (Grants No. 02-02-17062 and 03-02-16626), and Russian State Program on Superconductivity (Project No. 40.012.1.1.11.46).

*E-mail address: uspenska@issp.ac.ru
†E-mail address: alrakhmanov@mail.ru

[1] E.H. Brandt, Rep. Prog. Phys. **58**, 1465 (1995).
[2] D. Feinberg, J. Phys. III **4**, 169 (1994).
[3] G. Blatter, M.V. Feigel'man, V.B. Geshkenbein, and V.M. Vinokur, Rev. Mod. Phys. **66**, 1125 (1994).
[4] D.T. Fuchs, E. Zeldov, D. Majer, R.A. Doyle, T. Tamegai, S. Ooi, and M. Konczykowski, Phys. Rev. B **54**, 796 (1996).
[5] A.E. Koshelev, Phys. Rev. Lett. **83**, 187 (1999).
[6] M. Baziljevich, D. Giller, M. McElfresh, Y. Abulafia, Y. Radzyner, J. Schneck, T.H. Johansen, and Y. Yeshurun, Phys. Rev. B **62**, 4058 (2000).
[7] M.J.W. Dodgson, cond-mat/0201197 (unpublished).
[8] A. Soibel, E. Zeldov, M. Rappoport, Yu. Myasoedov, T. Tamegai, S. Ooi, M. Konczyakowski, and V.B. Geshkenbein, Nature (London) **406**, 282 (2000).
[9] N. Avraham, B. Khaykovich, Yu. Myasoedov, M. Rappoport, H. Shtrikman, D.E. Feldman, T. Tamegai, P.H. Kes, Ming Li, M. Konczyakowski, Kees van der Beek, and E. Zeldov, Nature (London) **411**, 451 (2001).
[10] A. Schilling, R. Jin, J.D. Guo, and H.R. Ott, Phys. Rev. Lett. **71**, 1899 (1993).
[11] R. Cubitt, E.M. Forgan, G. Yang, S.L. Lee, D. McPaul, H.A. Mook, M. Yethiraj, P.H. Kes, T.W. Li, A.A. Menovsky, Z. Tarnawski, and K. Mortensen, Nature (London) **365**, 407 (1993).

[12] K. Harada, T. Matsuda, H. Kasai, J.E. Bonevich, T. Yoshida, U. Kawabe, and A. Tonomura, Phys. Rev. Lett. **71**, 3371 (1993).
[13] S.L. Lee, P. Zimmermann, H. Keller, M. Warden, I.M. Savic, R. Schauwecker, D. Zech, R. Cubitt, E.M. Forgan, P.H. Kes, T.W. Li, A.A. Menovsky, and Z. Tarnawski, Phys. Rev. Lett. **71**, 3862 (1993).
[14] Ch. Joss, J. Albrecht, H. Kuhn, S. Leonard, and H. Kronüller, Rep. Prog. Phys. **65**, 1651 (2002).
[15] V. K. Vlasko-Vlasov, U. Welp, G. W. Crabtree, and V. I. Nikitenko, in *Physics and Material Science of Vortex States, Flux Pinning and Dynamics*, Vol. 356 of *NATO Advanced Study Institute, Series E: Applied Sciences*, edited by R. Kossowvsky *et al.* (Kluwer Academic Publishers, Dordrecht, 1999), pp. 205–237.
[16] M.V. Indenbom, A. Forkl, B. Ludescher, H. Kronüller, H.-U. Habermeier, B. Leibold, G. D'Anna, T.W. Li, P.H. Kes, and A.A. Menovsky, Physica C **226**, 325 (1994).
[17] V.K. Vlasko-Vlasov, A. Koshelev, U. Welp, G.W. Crabtree, and K. Kadowaki, Phys. Rev. B **66**, 014523 (2002).
[18] A. Grigorenko, S. Bending, T. Tamegai, S. Ooi, and M. Henini, Nature (London) **414**, 728 (2001).
[19] T. Matsuda, O. Kamimura, H. Kasai, K. Harada, T. Yoshida, T. Akashi, A. Tonomura, Y. Nakayma, J. Shimoyama, K. Kishio, T. Hanaguri, and K. Kitazawa, Science **294**, 2136 (2001).
[20] M. Yasugaki, K. Itaka, M. Tokunaga, N. Kameda, and T. Tamegai, Phys. Rev. B **65**, 212502 (2002).
[21] M. Tokunaga, M. Kobayashi, Y. Tokunaga, and T. Tamegai, Phys. Rev. B **66**, 060507 (2002).
[22] P.H. Kes, J. Aarts, V.M. Vinokur, and C.J. van der Beek, Phys. Rev. Lett. **64**, 1063 (1990).
[23] E.H. Brandt, Phys. Rev. Lett. **68**, 3769 (1992).
[24] M. Bou-Diab, M.J.W. Dodgson, and G. Blatter, Phys. Rev. Lett. **86**, 5132 (2001).
[25] A. M. Campbell and J. E. Evetts, *Critical Currents in Superconductors* (Taylor and Francis, London, 1972).
[26] E.H. Brandt, Phys. Rev. B **25**, 5756 (1982).
[27] A. Perez-Gonzalez and J.R. Clem, Phys. Rev. B **31**, 7048 (1985).
[28] M.A.R. LeBlanc, S. Celebi, S.X. Wang, and V. Plechacek, Phys. Rev. Lett. **71**, 3367 (1993).
[29] M.V. Indenbom, C.J. van der Beck, V. Berseth, W. Benoit, G. D'Anna, A. Erb, E. Walker, and R. Fluekiger, Nature (London) **385**, 702 (1997).
[30] L.N. Bulaevskii, M. Maley, H. Safar, and D. Dominguez, Phys. Rev. B **53**, 6634 (1996).
[31] S.E. Savel'ev, J. Mirkovic, and K. Kadowaki, Phys. Rev. B **64**, 094521 (2001).
[32] F.X. Rei, J. Schneck, H. Savary, R. Mellet, and C. Daguet, Appl. Supercond. **1**, 627 (1993).
[33] I. Chong, Z. Hiroi, M. Izumi, J. Shimoyama, Y. Nakayama, K. Kishio, Y. Nakayama, T. Terashima, Y. Bando, and M. Takano, Science **276**, 770 (1997).
[34] J. Shimoyama, K. Murakami, K. Shimizu, Y. Nakayama, and K. Kishio, Physica C **357-360**, 1091 (2001).
[35] T. Motohashi, Y. Nakayama, T. Fujita, K. Kitazawa, J. Shimoyama, and K. Kishio, Phys. Rev. B **59**, 14 080 (1999).
[36] A.B. Kulakov, I.K. Bdikin, S.A. Zver'kov, G.A. Emel'chenko, G. Yang, and J.S. Abell, Physica C **371**, 45 (2002).
[37] A.B. Kulakov, I.G. Naumenko, S.A. Zver'kov, A.V. Kosenko, S.S. Khasanov, I.K. Bdikin, G.A. Emel'chenko, M. Fehlman, L.J. Gaukler, G. Yang, and J.S. Abell, J. Cryst. Growth **371**, 194 (2001).
[38] L.A. Dorosinskii, M.V. Indenbom, V.I. Nikitenko, Yu.A. Ossip'ian, A.A. Polyansky, and V.K. Vlasko-Vlasov, Physica C **203**, 149 (1992).
[39] L.S. Uspenskaya, V.K. Vlasko-Vlasov, V.I. Nikitenko, and T.H. Johansen, Phys. Rev. B **56**, 11 979 (1997).
[40] L.S. Uspenskaya, A.B. Kulakov, and A.L. Rakhmanov, Pis'ma Zh. Eksp. Teor. Fiz. **76**, 213 (2002) [JETP Lett. **76**, 180 (2002)].
[41] D.S. Fisher, Phys. Rev. B **22**, 1190 (1980).
[42] M.V. Feigelman, V.B. Geshkenbein, and A.I. Larkin, Physica C **167**, 177 (1990).